Role of Ribosomal Protein L27 in Peptidyl Transfer[†]

Stefan Trobro and Johan Åqvist*

Department of Cell and Molecular Biology, Uppsala Biomedical Center, Uppsala University, Box 596, SE-751 24 Uppsala, Sweden

Received February 1, 2008; Revised Manuscript Received March 3, 2008

ABSTRACT: The current view of ribosomal peptidyl transfer is that the ribosome is a ribozyme and that ribosomal proteins are not involved in catalysis of the chemical reaction. This view is largely based on the first crystal structures of bacterial large ribosomal subunits that did not show any protein components near the peptidyl transferase center (PTC). Recent crystallographic data on the full 70S ribosome from *Thermus thermophilus*, however, show that ribosomal protein L27 extends with its N-terminus into the PTC in accordance with independent biochemical data, thus raising the question of whether the ribozyme picture is strictly valid. We have carried out extensive computer simulations of the peptidyl transfer reaction in the *T. thermophilus* ribosome to address the role of L27. The results show a reaction rate similar to that obtained in earlier simulations of the *Haloarcula marismortui* reaction. Furthermore, deletion of L27 is predicted to only give a minor rate reduction, in agreement with biochemical data, suggesting that the ribozyme view is indeed valid. The N-terminus of L27 is predicted to interact with the A76 phosphate group of the A-site tRNA, thereby explaining the observed impairment of A-site substrate binding for ribosomes lacking L27. Simulations are also reported for the reaction with puromycin, an A-site tRNA analogue which lacks the A76 phosphate group. The calculated energetics shows that this substrate can cause a downward pK_a shift of L27 and that the reaction proceeds faster with the L27 N-terminus deprotonated, in contrast to the situation with aminoacyl-tRNA substrates. These results could explain the observed differences in pH dependence between the puromycin and C-puromycin reactions, where the former reaction has been seen to depend on an additional ionizing group besides the attacking amine, and our model predicts this ionizing group to be the N-terminal amine of L27.

The genetic code is translated from mRNA into protein sequence by the ribosome, a macromolecular complex consisting of a small and a large subunit that contain rRNA chains (rRNA) and ~50 proteins. During mRNA translation, the C-terminal end of the growing peptide is ester bonded to the universal CCA O3′ terminus of a tRNA molecule (peptidyl-tRNA) in the ribosomal P-site. For the next amino acid to become attached to the growing chain, the cognate aminoacyl-tRNA (aa-tRNA) molecule to be selected is delivered to the ribosomal A-site in a ternary complex with elongation factor EF-Tu and GTP. In peptide chain elongation, the α-amino group of the incoming aa-tRNA attacks the carboxyl carbon of the peptidyl-tRNA ester, and the reaction also requires deprotonation of the nucleophile and protonation of the leaving P-site tRNA 3′-ribose oxygen. The peptide chain thus becomes ester bonded to the A-site tRNA and contains the new amino acid at its C-terminus. Selection of the cognate aa-tRNA takes place at the mRNA-programmed ribosomal decoding center on the small subunit (*1*). Here, the tRNA anticodon base pairs with the corresponding mRNA codon, while the other ends of the A- and P-site tRNAs meet at the peptidyl transferase center (PTC)[1] on the large subunit (*2, 3*), where the new peptide bond is formed. Translocation subsequently takes place by the action of elongation factor EF-G, where the ribosome slides a distance of three nucleotides relative to the mRNA, placing the former A-site tRNA in the P-site and the former P-site tRNA in the E-site, thus presenting an empty A-site with a new codon to be read in the next elongation cycle.

The high-resolution structure of the full 70S bacterial ribosome (*4*) complete with mRNA and tRNA and the previously published structures of the 50S subunit with and without tRNA analogues (*3, 5–9*) give a unified view of the position and structure of the peptidyl transferase center on the ribosome. The reacting aa-tRNA and peptidyl-tRNA groups are surrounded by ribosomal bases A2602, C2063, A2451, U2585, and U2506 (*Escherichia coli* numbering), and no conserved metal ion is found close to the PTC in a position enabling it to participate in peptidyl transfer. The high-resolution 50S structures show no ordered protein close to the PTC, while the recent *Thermus thermophilus* 70S high-resolution structure (*4*) reveals that the N-terminus of ribosomal protein L27 extends from its globular domain into the PTC (Figure 1). This raises the question of whether L27 contributes to the catalysis of peptidyl transfer. As judged from structures of the archaeal *Haloarcula marismortui* large subunit, which lacks L27 or any homologous counterpart, the ribosomal PTC has so far been regarded as a true ribozyme (*5, 6, 10, 11*).

[†] This work was supported by a grant from the Swedish Research Council (VR).

* To whom correspondence should be addressed. Phone: +46 18 471 4109. Fax: +46 18 536971. E-mail: aqvist@xray.bmc.uu.se.

[1] Abbreviations: PTC, peptidyl transferase center; Pmn, puromycin; MD, molecular dynamics; EVB, empirical valence bond; FEP, free energy perturbation.

10.1021/bi8001874 CCC: $40.75
Published on Web 04/08/2008

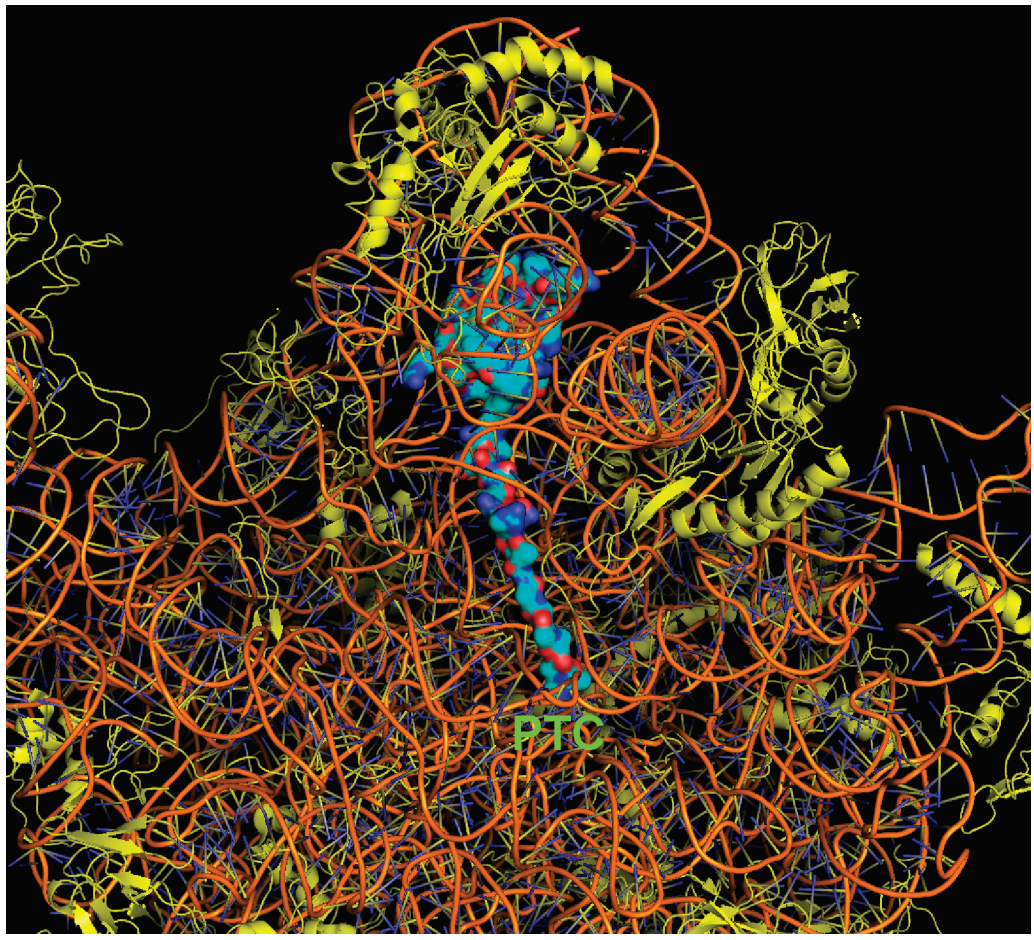

FIGURE 1: Illustration of how L27 reaches into the peptidyl transferase center (PTC). Part of the large ribsomal subunit from the *T. thermophilus* 70S structure (*4*) is shown with the L27 protein surface highlighted (carbons colored cyan).

The catalytic effect and mechanism of peptidyl transfer in the PTC have been investigated by fast pre-steady state kinetics showing that the PTC catalyzes peptidyl transfer by reducing the activation entropy compared to that of the corresponding uncatalyzed water reaction (*12*). It has further been shown that chemical modification of P-site A76 O2′ to H or F removes the catalytic activity of the PTC (*13, 14*) and that replacing the A2451 2′-OH group with H also has a deleterious effect (*15, 16*). In contrast, mutations of several bases in the "inner shell" around the reactants do not reduce the peptidyl transfer rate when full-length tRNA or analogues containing C75 or more are used as A-site substrates (*17, 18*), with the exception of the A2450G/C2063U double mutation (*19*). The critical effect of P-site A76 O2′ and the fact that it is within hydrogen bonding distance of the A-site α amino group (*6, 9, 14*) strongly suggest that the proton transfer is mediated via the P-site A76 O2′ (*10, 14*). The origin of the catalytic effect is, however, not confined to the substrates themselves since they or their analogues react no faster in water than regular esters (*12, 20–22*). Furthermore, no pH dependence on ribosomal groups is observed in fast quenched-flow measurements of the peptidyl transfer rate, when full-length tRNA or analogues containing C75 or more are used as A-site substrates (*23–25*). A pH−rate profile with a slope >1 would be expected for the bare chemical step if a ribosomal base takes part in the proton transfers and the attacking amino group ionizes at a pH value between 6 and 8.

The experimental data on the peptidyl transfer reaction were rationalized by computer simulations, where the reaction mechanism involving A-site A76 O2′ as a proton shuttle was found to be significantly catalyzed by the PTC (*10, 11, 20*). Catalysis is mainly achieved through a stable network of hydrogen bonds to the reactants that reduces the reorganization energy and activation entropy loss associated with the reaction. This predicted hydrogen bonding network (*10, 11*), including positions of key solvent molecules and the stereochemical route of the peptidyl transfer reaction, was later verified by new crystal structures with transition state analogues (*8, 9*). The other reaction catalyzed by the PTC together with ribosomal release factors, namely hydrolysis of the peptidyl-tRNA bond in translation termination, has also recently been predicted to proceed by a similar mechanism (*26*).

Zimmermann and co-workers (*27*) have shown that deletion mutants of *E. coli* lacking L27 have a phenotype with severe growth defects (5−6 times slower) and high temperature sensitivity. Photochemical cross-linking also showed that the A-site A76 nucleobase is in the proximity of L27 (*28*), and slow pre-steady state kinetics, using the minimum aa-tRNA analogue puromycin as the A-site substrate, measured 3−4 times slower peptidyl transfer for 70S-mutated ribosomes from which L27 has been removed (*27*). Moreover, the ability to bind A-site tRNA was significantly weakened in 70S-mutated ribosomes lacking L27, while the P-site binding was unaffected. This led to the suggestion that

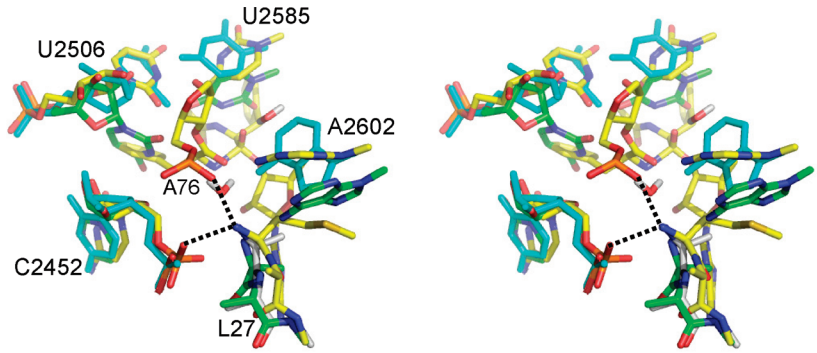

FIGURE 2: Structure of the PTC with L27 present. A representative MD structure along the reaction path toward the transient tetrahedral intermediate is shown with yellow carbons, where hydrogen bonding between the N-terminus of L27 and the A-site A76 and C2451 phosphates is indicated. The corresponding position of L27 in simulations employing a polyalanine model of the protein is shown with white carbons. The *T. thermophilus* structure (*4*), with no A-site substrate in the PTC but with L27 present, is drawn with green carbons. Relevant parts of the induced *H. marismortui* 1VQN structure (*8*), which lacks L27, is shown for comparison in cyan.

L27 interacts with the 3′-end of the A-site tRNA to promote binding (*27*). These findings were later confirmed, and the effects were located to the N-terminal end of L27. That is, ribosomes lacking the three first amino acids of the L27 N-terminus did not cross-link to the tRNA 3′-end and showed reduced peptidyl transferase activity with puromycin as the A-site substrate (*29*), suggesting that the N-terminus of L27 reaches into the PTC. This was finally confirmed in the 70S 2.8 Å structure from *T. thermophilus* (*4*) where a weak density from residues 1–9 allowed the N-terminal backbone of L27 to be resolved, but no density for the 3′-end of the A-site tRNA was visible.

To investigate the interactions between the L27 N-terminus and the reactants (especially the A-site tRNA), we have carried out new computer simulations of the peptidyl transfer reaction, employing the 2.8 Å *T. thermophilus* structure as starting coordinates. It should be pointed out that in the recently published 3.7 Å structure of the 70S *T. thermophilus* ribosome (*30*) no density was observed for the first nine residues of L27; therefore, we will consider only the higher-resolution structure (*4*) herein. Free energy barriers and corresponding reaction rates were calculated, and the key interactions analyzed, for several relevant cases. These include the different protonation states of the L27 N-terminal amine, the mutated ribosome that lacks L27, and the peptidyl transfer reaction with both aa-tRNA and puromycin as the A-site substrate.

MATERIALS AND METHODS

The rRNA and L27 coordinates from the 70S *T. thermophilus* structure with Protein Data Bank (PDB) entry 2J01 and ions from PDB entry 2J00 (*4*) were superimposed on the *H. marismortui* 50S structure (PDB entry 1VQN) (*8*), after aligning the phosphate atoms of residues 2400–2600 (*E. coli* numbering) in 1VQN to 2J01. This was done to obtain accurate tRNA coordinates from 1VQN, since no A-site tRNA density was observed in the PTC for the 70S structure and since the P-site tRNA in that case was deacylated. In total, 169 phosphate atoms were aligned with an average root-mean-square (rms) deviation of 1.1 Å. The A-site 5′-CC-PPU-3′-LOF molecule from 1VQN was converted to 5′-CCA-3′-Phe, and the P-site 5′-CCA-3′-Phe-ACA-BTN molecule from 1VQN was converted to 5′-CCA-3′-Phe-Gly with a neutral Gly N-terminus. The 2J01 coordinates for U2506 were replaced by the corresponding aligned coordinates from 1VQN (cf. Figure 2), to attain an "induced conformation" (*8*) that could accommodate the substrates (which are not not present in the 2J00–2J01 structure), and the C1′−N9 bonds of U2506 and U2585 were rotated to prevent steric clashes with the substrates. Two different models of the L27 N-terminal tail were used (see Results), one in which the side chains of the first three residues were explicitly modeled from the crystallographic C_β coordinates and a second corresponding to the polyalanine model deposited in the PDB (*4*).

The side chains of the first nine residues of L27 in the *T. thermophilus* structure (*4*) are not visible in the electron density and were modeled crystallographically as polyanalanine, while the model is complete from Thr10 and onward (*4*). Hence, while a nine-residue polyalanine chain from the N-terminus to the first well-defined side chain (Thr10) was refined crystallographically, the possibility remains that Met1 is post-translationally lost and that an eight-residue chain starting with Ala2 could perhaps also be refined into the observed density (M. Selmer, personal communication). To take both of these sequence possibilities into account, we constructed two different models of L27. In the first model, the first three amino acids of the N-terminus were modeled with side chains as Met-Ala-His after the C_β coordinates in 2J01, while the following two lysine residues were converted to alanines since there is no information about their side chain positions and they are far from the reacting groups. In the second model, we simply retained a polyalanine chain (the first residue is Ala in case the Met is cleaved off) and applied weak (1 kcal mol^{-1} Å^{-2}) harmonic positional restraints to the backbone atoms in the simulations. The two models turn out to give very similar energetic results, since the main effect of L27 appears to come from the terminal amino group (see below), and most of the presented results were obtained with the first model.

For each of the different reaction simulations, a solvated spherical system with a 20 Å radius centered on the P-site carbonyl carbon atom was set up for molecular dynamics free energy perturbation simulations as described previously (*10, 11*). The MD simulations were performed with Q (*31*) using the Charmm22 force field (*32*) and a time step of 1 fs. Atoms within the 20 Å system were fully mobile; those outside the system boundary were restrained to their initial positions with a 100 kcal mol^{-1} Å^{-2} harmonic force constant, and nonbonded interactions across the system boundary were

not calculated. Ionic groups within 5 Å of the system boundary were neutralized as described previously (*10*). Water molecules close to the sphere boundary were restrained to reproduce the correct density and polarization (*31*). All nonbonded interactions within the 20 Å system were calculated for the reacting groups, while other interactions were treated with a 10 Å cutoff together with a multipole expansion of long-range electrostatics (*33*).

The peptidyl transfer reaction free energy surface was treated with the empirical valence bond (EVB) method (*34, 35*) and described by three resonance structures, corresponding to reactants (R), a transient tetrahedral intermediate (TI), and products (P), with calibration of the uncatalyzed water reaction energetics as described previously (*10*). Reaction free energy profiles in water and in the solvated ribosome model were calculated with the free energy perturbation/umbrella sampling method (*34, 35*). Each free energy perturbation (FEP) calculation comprised 80 discrete steps, with a trajectory of 5–20 ps generated at each step, and covered a path going from pure reactants to products via a state with weights of 20, 60, and 20% for R, TI, and P, respectively. The reason for using a more concerted FEP pathway is that the actual ground state of the reaction, resulting from mixing of the EVB resonance structures, lies closer to this path and the sampling may be thus be improved (*26*). The system in each simulation was initially heated in this state according to a stepwise protocol from 0 to 300 K and then equilibrated for 2–8 ns at 300 K before trajectories were propagated toward reactants and products. Each free energy perturbation simulation was also repeated at least three times with different initial conditions.

RESULTS

Peptidyl Transfer to aa-tRNA with L27 Present. The structure of the PTC and the hydrogen bonding network observed in the MD simulations of the reaction using the *T. thermophilus* structure (*4*) are in general very similar to the earlier *H. marismortui* simulations (*10, 11*). However, a notable difference is that the N-terminal amine of L27 interacts with the phosphate esters of the A-site A76 and C2452, thus forming an ionic triad with these two phosphate groups (Figure 2). An additional hydrogen bond to the L27 amine is also provided by the water molecule located between the A-site substrate carbonyl group and O2′ of A2451 (*8, 11*). The MD simulations result in only minor structural changes compared to the crystal structure (*4*). The U2585 base that initially covers the substrate ester moves away (Figure 2) from the P-site 3′-ester carbonyl group to accommodate the oxyanion intermediate as previously observed in *H. marismortui* 50S structures, containing an A-site acylated CCA substrate or transition state analogue (*8*), and in earlier calculations (*10, 11*). This movement is part of the induced fit model suggested by Schmeing et al. (*8*), where the ester carbonyl group is brought into an active conformation by binding of the CCA sequence to the A-site. U2506 remains in the position it has in the "induced" structure rather than reverting back to the 70S *T. thermophilus* structure, due to the presence of the A-site substrate.

The formation of the L27 ion pairs is accompanied by only small structural changes in the L27 backbone compared to the crystal structure. The eclipsed Cβ−Cα−C−O torsion angle of Ala2 in L27 is relaxed by rotation of Cβ toward A2602. The Met1 side chain moves toward A2602 and displaces this base slightly toward the A-site, i.e., to a position closer to that observed in the induced 50S structure (Figure 2). In simulations with the polyalanine model of L27, a similar movement of the Ala1 side chain can be observed (Figure 2) that also results in a slight displacement of A2602 in the same directions as with Met in the first position (not shown). It is also noteworthy that the ionic triad emerges already after superpositioning of the *H. marismortui* and *T. thermophilus* structures, with initial nitrogen−phosphate oxygen distances of 3.6 and 4.0 Å to A76 and C2452, respectively. In the case of the 1VQ7 *H. marismortui* structure containing a transition state analogue (*8*), a magnesium ion is also found to occupy the position where the L27 N-terminal amino group is located in the *T. thermophilus* structure. Taken together, the data described above therefore clearly indicate a strong propensity for positive charge between the phosphates of the A-site A76 and C2452.

The activation free energy for peptidyl transfer to an aminoacylated tRNA substrate in the *T. thermophilus* PTC is calculated to be 16.1 ± 1.1 kcal/mol, yielding a predicted rate of ∼10 s^{-1} at 300 K using standard transition state theory. Furthermore, the difference in activation barrier between the possible cases where L27 has either a Met or an Ala residue in the first position is within the error bars of the calculations (the polyalanine model gives a barrier of 15.5 kcal/mol). These results are very similar to those predicted earlier for the *H. marismortui* 50S subunit (*10, 11*) and thus yield a rate acceleration of ∼1 million compared to the uncatalyzed water reaction (Figure 3). The simulation results are also in agreement with the rates measured at physiological pH on 50S or 70S ribosomes with quenched flow using puromycin (Pmn) or C-Pmn as the A-site substrate (*12, 21, 24*).

Peptidyl Transfer with L27 Removed. To examine the effect of L27 on the catalytic process, we carried out multiple simulations of the peptidyl transfer reaction with L27 deleted from the ribosome, thus allowing more water to approach the PTC through the empty space that is created. These calculations predict a relatively small effect of L27 on the activation free energy of the reaction, with the barrier increased by only 1.3 kcal/mol to a total of 17.4 kcal/mol (Figure 3), corresponding to a rate decrease by a factor of 10. It is clearly encouraging that this rate decrease agrees well with that found experimentally (*27*), although the predicted effect is similar in magnitude to the error bars of the calculations. It thus seems clear that L27 is not a major contributor to the overall catalytic effect of ∼1 million.

In the simulations of the mutant ribosome lacking L27, several additional water molecules enter the space created by removal of the protein as expected (Figure 4). Furthermore, the simulations generally show an increased mobility in the PTC when L27 is absent. The U2506 base tilts up toward G2583 and interacts with this base (Figure 4) in a manner similar to that of the 50S *H. marismortui* structure with sparsomycin in the A-site (*6*), while A2602 retains the position it has in the 70S *T. thermophilus* structure. The A-site A76 base moves slightly toward the oxyanion, thereby displacing the ribose backbone of U2584–U2585 toward G2608, while the C75 base pairing with G2553 is maintained. The P-site CCA-peptidyl part interacts with the rRNA as in

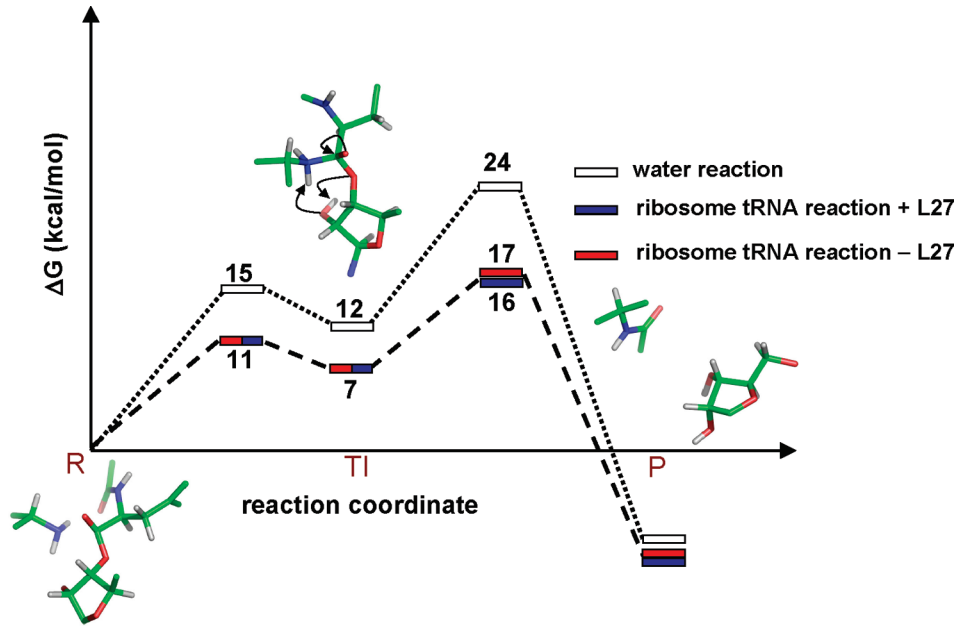

FIGURE 3: Calculated free energy profiles for the uncatalyzed peptidyl transfer reaction in solution and for the *T. thermophilus* ribosome reaction with aa-tRNA as the A-site substrate, with and without L27 present (average error bars for the FEP calculations are ±1.1 kcal/mol). R, TI, and P denote reactants, the tetrahedral intermediate, and products, respectively.

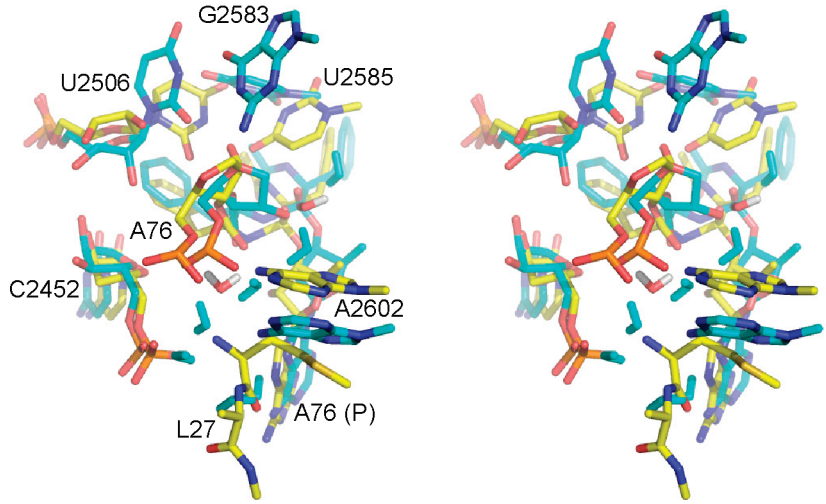

FIGURE 4: Comparison of MD structures of the transient tetrahedral intermediate with (yellow carbons) and without (cyan carbons) L27 present. Water molecules in the latter structure are also colored cyan.

the 70S *T. thermophilus* crystal structure and is apparently unaffected by the removal of L27. This is also in accord with experimental data showing that L27 does not affect P-site tRNA binding (*27*). One may also note the presence in Figure 4 of the water molecule interacting with the negative substrate ester carbonyl oxygen, in simulations both with and without L27, and this water molecule appears to be a conserved feature of the reaction observed both in MD simulations (*10, 11, 26*) and in crystal structures with transition state analogues (*9*).

The ion pair between the L27 N-terminus and the A-site A76 phosphate ester gives a straightforward explanation for the reduced binding affinity of aa-tRNA in the A-site when L27 is removed from the PTC and confirms the prediction that L27 interacts with and helps in positioning the A-site aa-tRNA during peptidyl transfer (*27*). It is also in line with the observation that C-Pmn is more tightly bound to the PTC than Pmn (*24*), since Pmn lacks a negatively charged phosphate ester and thus cannot make an ion pair with the L27 N-terminus. The presence of the C75 base in C-Pmn most likely also contributes to its significantly lower K_d value. The interaction between the positively charged L27 N-terminus and the phosphates of A76 and C2452 strongly suggests that the pK_a of the NH_3^+ group is at least not shifted downward from its normal value of 9–10. Hence, in the pH range of 6–8 where ribosome kinetics has typically been measured, one would not expect ionization of L27 to show up in pH−rate profiles. This is consistent with the interpretation that only the attacking amino group ionization strongly affects the rate when C-Pmn and CC-Pmn are used as substrates (*24, 25*). The lack of pH dependence for full-length aa-tRNA substrates (*23*), on the other hand, is most easily rationalized by a rate-limiting step other than peptidyl transfer (such as accommodation) which masks the ionization of the attacking amino group.

Peptidyl Transfer with Puromycin as the A-Site Substrate. The situation is apparently different with Pmn as the A-site substrate, in which case a second ionizing group with a pK_a

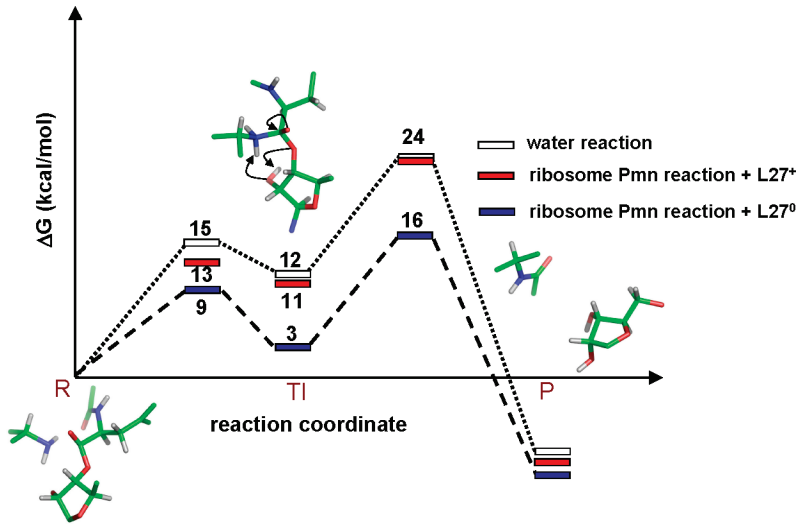

FIGURE 5: Calculated free energy profiles for the uncatalyzed peptidyl transfer reaction in solution and for the *T. thermophilus* ribosome reaction with puromycin (Pmn) as the A-site substrate, with the L27 N-terminus either protonated ($L27^+$) or deprotonated ($L27^\circ$).

of ~7.5–8 has been observed in pH−rate profiles both for *E. coli* and for *Mycobacterium smegmatis* ribosomes (*18, 24, 25*). From our discussion of the interaction between the L27 N-terminus and the A76 phosphate group, it would appear that if the A-site substrate lacks this phosphate, which is the case with puromycin, the pK_a of L27 could be shifted downward so that the NH_3^+ deprotonation now shows up in the pH dependence of the reaction. To address this issue, we carried out simulations of peptidyl transfer with Pmn as the A-site substrate, both with the L27 N-terminus protonated and deprotonated and with L27 removed.

For the Pmn reaction with a protonated, positively charged L27 amino group, the peptidyl transfer free energy barriers obtained from MD/FEP/EVB simulations are 23.5 kcal/mol (Figure 5), a value which is significantly higher than in calculations with aa-tRNA as the A-site substrate. The corresponding rate would be on the order of only 10^{-5} s^{-1}, i.e., the same as for the uncatalyzed reaction in water, implying essentially no catalytic effect of the ribosome. The situation, however, changes drastically when the L27 amino group is deprotonated; the calculated activation free energy then decreases to 16.1 ± 0.6 kcal/mol (Figure 5), which is in good agreement with experimental data (*18, 24, 25*) and with our simulations of the reaction with aa-tRNA. Furthermore, complete removal of L27 from the system causes an only minor increase in the activation free energy for the Pmn reaction to 16.5 ± 1.2 kcal/mol (data not shown) which appears consistent with the results of Maguire et al. (*29*).

For the faster rate of peptidyl transfer to Pmn to be operational in native ribosomes (Figure 5), a downward pK_a shift of L27 is required so that the deprotonated form of the N-terminus is present at a sufficient concentration during the reaction. We examined the possibility of such a shift by carrying out FEP simulations of the process of transforming the L27 NH_3^+ group to an NH_2 group in the presence of both Pmn and aa-tRNA in the A-site, which will yield an estimate of the corresponding pK_a shift. These calculations indicate that the protonated form of L27 is destabilized by 2.5 kcal/mol when Pmn is bound to the A-site instead of aa-tRNA, which is equivalent to a pK_a shift of approximately −2. Calculations of absolute pK_a values inside biological macromolecules are still very challenging and often associated with large errors; however, the estimation of pK_a shifts is generally more reliable (*36*), and the prediction of a downward shift is thus expected to be significant.

The simulations of the puromycin reaction thus yield a picture in which binding of Pmn to the A-site shifts the pK_a of L27 so that the N-terminus now is deprotonated at a lower pH. With an aa-tRNA substrate, the pK_a of L27 could very well also be shifted upward from its normal value in solution due to the ionic interaction. We therefore propose that the L27 amine could be the elusive ionizable ribosomal group with a measured pK_a of ~7.5–8 in the Pmn reaction. This effect is then mainly attributed to the lack of the A76 phosphate group in Pmn, which is present in both C-Pmn and aa-tRNA substrates. Apparently, the phosphate group of C2452 alone is not sufficient to stabilize the protonated form of L27, which is also suggested by the fact that the MD simulations show a weakened interaction in which C2452 is not able to hold the protonated N-terminus in a well-defined position. This model would thus also predict the pH dependence on the additional ribosomal group to disappear when mutant ribosomes lacking L27 are measured. Likewise, synthetic A-site substrates carrying C75 or more but with the A76 phosphate ester replaced with a neutral linker would be predicted to exhibit impaired A-site substrate binding.

The adenine base of the Pmn substrate shows an increased mobility in all MD simulations of the Pmn reaction, which is not surprising since the lacking A-site C74 and C75 bases normally would contribute to holding the A-site substrate in place. However, the structure of the PTC is generally very similar to the simulations with aa-tRNA in the A-site, supporting the notion that Pmn is a good model substrate for the native peptidyl transfer reaction. The simulations also show that the position and conformation of Pmn are further stabilized by interactions involving U2506 and U2585, where the former uracil base can accept a hydrogen bond from the puromycin-specific NH linker that replaces the normal tRNA ester bond (Figure 6). A major difference in the Pmn reaction is, however, that the ionic interaction between the A76 phosphate and L27 is missing. The position of the L27 N-terminus is generally less well-defined in the simulations with Pmn, particularly for the case with a neutral N-terminus

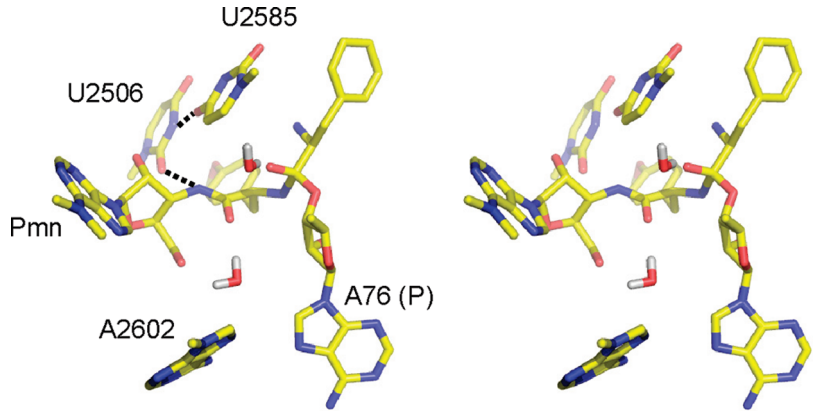

FIGURE 6: Representative snapshot from MD simulations of the Pmn reaction, with a neutral L27 N-terminus, in the approach toward the transient tetrahedral intermediate. Key hydrogen bonds involving U2506 and U2585 are indicated.

where it spans a range of conformations. It thus seems possible that the lack of strong electron density for the L27 N-terminus in the crystal structure with no substrate in the A-site (*4*) could be a consequence of the missing interaction with A76. In view of the weak experimental density for the N-terminus, it is not meaningful to try to draw conclusions about its protonation state in the crystals, but one can note that its shortest interaction distance (2.7 Å) is with the N6 amino group of A2602, which would indicate that the N-terminus is a hydrogen bond acceptor and hence neutral. In this context, it also appears logical that mutations of key nucleotides surrounding the A-site substrate, such as U2506, U2585, and A2602, can have a more pronounced effect on the Pmn reaction than with C-Pmn or aa-tRNA as the substrate (*24*). That is, the relative importance of these bases in sequestering the Pmn substrate is likely to be enhanced when both C75 and the L27 interaction are missing. In particular, it appears that hydrogen bonding between U2506 and the NH linker of Pmn (Figure 6) could be critical so that mutation of this nucleotide is likely to significantly destabilize the bound conformation of Pmn (*24*).

DISCUSSION

The finding that ribosomal protein L27 extends into the peptidyl transferase center and makes contact with the tRNA substrates (*4, 27, 29*) seems to challenge the view that the ribosome is a ribozyme. Here, we have addressed the role of L27 in the peptidyl transfer reaction by computer simulations that have earlier proven to yield reliable results for the ribosome, with respect to both energetics and structure (*10, 11*). These simulations predict that the catalytic rate constant for peptidyl transfer is reduced by a factor of only 10 when L27 is removed from the ribosome. This result is basically in agreement with the experiments of Zimmermann and co-workers who found that both peptidyl transferase activity, as measured with puromycin, and bacterial growth are slowed by a similar factor (*27, 29*). Furthermore, our calculations point to the importance of the ionic interaction between the L27 N-terminus and the A-site A76 phosphate group for stabilizing the bound A-site substrate, again in agreement with the experimental finding that ribosomes lacking L27 are deficient in binding A-site, but not P-site, tRNAs (*27*). The effect of this interaction may also contribute to the considerably tighter binding to the PTC observed for C-Pmn, which has the A76 phosphate, compared to Pmn that lacks it (*24*). However, the overall catalytic effect on peptidyl transfer exerted by the ribosome corresponds to a rate enhancement of ~1 million (*12*), and this effect was reproduced both by earlier simulations of the reaction in the *H. marismortui* large subunit (*10, 11, 20*) and by the present reaction in the *T. thermophilus* ribosome. Hence, a factor of at most 10, due to the presence of L27 in the PTC, must be considered as a minor contribution compared to the total catalytic effect. In this sense, it does not seem warranted to question the ribosome's status as a ribozyme. An interesting issue is, of course, why bacteria still invest the cost of synthesizing a protein like L27 if it does not contribute more to the efficiency of peptidyl transfer. However, with L27 present, a significant increase in the bacterial growth rate has been demonstrated, and the protein also has effects on ribosome assembly and stability, as well as on peptidyl transfer rates (*27*).

An interesting question regarding L27 is also whether its terminal Met residue is post-translationally lost in *T. thermophilus*, as is the case with many bacterial proteins. The 70S crystal structure was refined with a polyalanine model of nine residues preceding the first residue (Thr10) with visible side chain density, since only weak density was observed for that part (*4*). While the crystal structure thus suggests that the Met residue is not lost, it might also be possible to refine the structure with a backbone model of only eight residues preceding Thr10 (M. Selmer, personal communication), in which case the chain would start with Ala2. In general, the loss of terminal Met residues from ribosomal proteins varies between different proteins and species, and while, for example, the human and *Rhodopseudomonas palustris* L27 species appear to retain the methionine (*37, 38*), it appears to be removed in *E. coli* (*39*). Ribosomal proteins from the *T. thermophilus* HB8 strain, used for crystallization of the 70S ribosome, have also been analyzed by mass spectrometry, but unfortunately, the results for L27 are somewhat ambiguous with respect to Met loss (*40*). In view of the apparent uncertainties regarding the actual N-terminal sequence that makes contact with the PTC in *T. thermophilus* (HB8) ribosomes, we carried out simulations for two different cases. First, we considered the N-terminal sequence Met-Ala-His (with side chains explicitly modeled) as indicated by the deposited PDB structure with a nine-residue backbone preceding Thr10 (*4*). Second, we retained a positionally restrained polyalanine chain in the

simulations, assuming that the first residue is Ala and that the entire segment preceding Thr10 could possibly be shortened by one residue by a straighter chain tracing. Interestingly, no significant difference was found in the calculated energetics for the aa-tRNA reaction between these two alternatives. This is consistent with our finding that it is the N-terminal amino group of L27 that makes the key interactions. The simulations also show that there is plenty of space to accommodate a possible methionine side chain in the first position without any really specific contacts with the rRNA.

We have also addressed the difference between the peptidyl transfer reactions with aa-tRNA and puromycin as A-site substrates. This was mainly motivated by the fact that Pmn appears to be an ideal model substrate that allows the bare chemical aminolysis step (peptidyl transfer) to be experimentally monitored without being masked by slower processes such as accommodation (*23*). However, an unexplained and curious feature of the Pmn reaction is the apperance of an additional ionizable group in the pH−rate profiles. Our prediction is that the Pmn reaction is only catalyzed by the ribosome, with L27 present in the PTC, if the L27 N-terminus is deprotonated and that this deprotonation may occur in the observed pH interval. This could thus explain the pH dependence of the Pmn reaction (*18, 24*). It would also explain the distinct difference in pH dependence between Pmn and C-Pmn (*24*), where the latter substrate contains the A76 phosphate group and thus does not trigger deprotonation of L27 (the same goes for aa-tRNA substrates, of course). Furthermore, complete removal of L27 in the Pmn reaction is predicted to yield an only minor decrease in the catalytic rate. Hence, if the conformation in which L27 is protruding into the PTC is in equilibrium (on a faster time scale than peptidyl transfer) with a "disordered" conformation akin to having L27 removed, these two situations would yield similar rates. Such a model could possibly provide an explanation for the fact that the slope of the pH−rate profile with Pmn is around 1.5 rather than 2 (*18, 24*).

ACKNOWLEDGMENT

We thank Drs. Marina Rodnina, Maria Selmer, and Måns Ehrenberg for useful comments.

REFERENCES

1. Ogle, J. M., and Ramakrishnan, V. (2005) Structural insights into translational fidelity. *Annu. Rev. Biochem. 74*, 129–177.
2. Ban, N., Nissen, P., Hansen, J., Moore, P. B., and Steitz, T. A. (2000) The complete atomic structure of the large ribosomal subunit at 2.4 Å resolution. *Science 289*, 905–920.
3. Harms, J., Schluenzen, F., Zarivach, R., Bashan, A., Gat, S., Agmon, I., Bartels, H., Franceschi, F., and Yonath, A. (2001) High resolution structure of the large ribosomal subunit from a mesophilic eubacterium. *Cell 107*, 679–688.
4. Selmer, M., Dunham, C. M., Murphy IV, F. V., Weixlbaumer, A., Petry, S., Kelley, A. C., Weir, J. R., and Ramakrishnan, V. (2006) Structure of the 70S ribosome complexed with mRNA and tRNA. *Science 313*, 1936–1942.
5. Nissen, P., Hansen, J., Ban, N., Moore, P. B., and Steitz, T. A. (2000) The structural basis of ribosome activity in peptide bond synthesis. *Science 289*, 920–930.
6. Hansen, J. L., Schmeing, T. M., Moore, P. B., and Steitz, T. A. (2002) Structural insights into peptide bond formation. *Proc. Natl. Acad. Sci. U.S.A. 99*, 11670–11675.
7. Schmeing, T. M., Seila, A. C., Hansen, J. L., Freeborn, B., Soukup, J. K., Scaringe, S. A., Strobel, S. A., Moore, P. B., and Steitz, T. A. (2002) A pre-translocational intermediate in protein synthesis observed in crystals of enzymatically active 50S subunits. *Nat. Struct. Biol. 9*, 225–230.
8. Schmeing, T. M., Huang, K. S., Strobel, S. A., and Steitz, T. A. (2005) An induced-fit mechanism to promote peptide bond formation and exclude hydrolysis of peptidyl-tRNA. *Nature 438*, 520–524.
9. Schmeing, T. M., Huang, K. S., Kitchen, D. E., Strobel, S. A., and Steitz, T. A. (2005) Structural insights into the roles of water and the hydroxyl of the P site tRNA in the peptidyl transferase reaction. *Mol. Cell 20*, 437–448.
10. Trobro, S., and Åqvist, J. (2005) Mechanism of peptide bond synthesis on the ribosome. *Proc. Natl. Acad. Sci. U.S.A. 102*, 12395–12400.
11. Trobro, S., and Åqvist, J. (2006) Analysis of predictions for the catalytic mechanism of ribosomal peptidyl transfer. *Biochemistry 45*, 7049–7056.
12. Sievers, A., Beringer, M., Rodnina, M. V., and Wolfenden, R. (2004) The ribosome as an entropy trap. *Proc. Natl. Acad. Sci. U.S.A. 101*, 7897–7901.
13. Dorner, S., Panuschka, C., Schmid, W., and Barta, A. (2003) Mononucleotide derivatives as ribosomal P-site substrates reveal an important contribution of the 2′-OH to activity. *Nucleic Acids Res. 31*, 6536–6442.
14. Weinger, J. S., Parnell, K. M., Dorner, S., Green, R., and Strobel, S. A. (2004) Substrate-assisted catalysis of peptide bond formation by the ribosome. *Nat. Struct. Mol. Biol. 11*, 1101–1106.
15. Erlacher, M. D., Lang, K., Shankaran, N., Wotzel, B., Hüttenhofer, A., Micura, R., Mankin, A. S., and Polacek, N. (2005) Chemical engineering of the peptidyl transferase center reveals an important role of the 2′-hydroxyl group of A2451. *Nucleic Acids Res. 33*, 1618–1627.
16. Erlacher, M. D., Lang, K., Wotzel, B., Rieder, R., Micura, R., and Polacek, N. (2006) Efficient ribosomal peptidyl transfer critically relies on the presence of the ribose 2′-OH at A2451 of 23S rRNA. *J. Am. Chem. Soc. 128*, 4453–4459.
17. Youngman, E. M., Brunelle, J. L., Kochaniak, A. B., and Green, R. (2004) The active site of the ribosome is composed of two layers of conserved nucleotides with distinct roles in peptide bond formation and peptide release. *Cell 117*, 589–599.
18. Beringer, M., Bruell, C., Xiong, L., Pfister, P., Bieling, P., Katunin, V. I., Mankin, A. S., Böttger, E. C., and Rodnina, M. V. (2005) Essential mechanisms in the catalysis of peptide bond formation on the ribosome. *J. Biol. Chem. 280*, 36065–36072.
19. Hesslein, A. E., Katunin, V. I., Beringer, M., Kosek, A. B., Rodnina, M. V., and Strobel, S. A. (2004) Exploration of the conserved A+C wobble pair within the ribosomal peptidyl transferase center using affinity purifies mutant ribosomes. *Nucleic Acids Res. 32*, 3760–3770.
20. Sharma, P. K., Xiang, Y., Kato, M., and Warshel, A. (2005) What are the roles of substrate-assisted catalysis and proximity effects in peptide bond formation by the ribosome? *Biochemistry 44*, 11308–11314.
21. Wohlgemuth, I., Beringer, M., and Rodnina, M. V. (2006) Rapid peptide bond formation on isolated 50S ribosomal subunits. *EMBO J. 7*, 699–703.
22. Guthrie, J. P. (1974) Hydration of carboxamides. Evaluation of the free energy change for addition of water to acetamide and formamide derivatives. *J. Am. Chem. Soc. 96*, 3608–3615.
23. Bieling, P., Beringer, M., Aido, S., and Rodnina, M. V. (2006) Peptide bond formation does not involve acid-base catalysis by ribosomal residues. *Nat. Struct. Mol. Biol. 13*, 423–428.
24. Brunelle, J. L., Youngman, E. M., Sharma, D., and Green, R. (2006) The interaction between C75 of tRNA and the A loop of the ribosome stimulates peptidyl transferase activity. *RNA 12*, 33–39.
25. Beringer, M., and Rodnina, M. V. (2007) Importance of tRNA interactions with 23S rRNA for peptide bond formation on the ribosome: Studies with substrate analogs. *Biol. Chem. 388*, 687–691.
26. Trobro, S., and Åqvist, J. (2007) A model for how ribosomal release factors induce peptidyl-tRNA cleavage in termination of protein synthesis. *Mol. Cell 27*, 758–766.
27. Wower, I. K., Wower, J., and Zimmerman, R. A. (1998) Ribosomal protein L27 participates in both 50S subunit assembly and the peptidyl transferase reaction. *J. Biol. Chem. 273*, 19847–19852.
28. Wower, J., Hixson, S. S., and Zimmerman, R. A. (1989) Labeling the peptidyltransferase center of the *Escherichia coli* ribosome with photoreactive $tRNA^{Phe}$ derivates containing azidoadenosine at the 3′ end of the acceptor arm: A model of the tRNA-ribosome complex. *Proc. Natl. Acad. Sci. U.S.A. 86*, 5232–5236.

29. Maguire, B. A., Beniaminov, A. D., Ramu, H., Mankin, A. S., and Zimmerman, R. A. (2005) A protein component at the heart of an RNA machine: The importance of protein L27 for the function of the bacterial ribosome. *Mol. Cell 20*, 427–435.
30. Korostelev, A., Trakhanov, S., Laurberg, M., and Noller, H. F. (2006) Crystal structure of a 70S ribosome-tRNA complex reveals functional interactions and rearrangements. *Cell 126*, 1065–1077.
31. Marelius, J., Kolmodin, K., Freierberg, I., and Åqvist, J. (1998) Q: A molecular dynamics program for free energy calculations and empirical valence bond simulations in biomolecular systems. *J. Mol. Graphics Modell. 16*, 213–225.
32. MacKerell, A. D., Wiórkiewicz-Kuczera, J., and Karplus, M. (1995) An all-atom empirical energy function for the simulation of nucleic acids. *J. Am. Chem. Soc. 117*, 11946–11975.
33. Lee, F. S., and Warshel, A. (1992) A local reaction field method for fast evaluation of long-range electrostatic interactions in molecular simulations. *J. Chem. Phys. 97*, 3100–3107.
34. Warshel, A. (1991) *Computer modeling of chemical reactions in enzymes and solutions*, John Wiley & Sons, New York.
35. Åqvist, J., and Warshel, A. (1993) Simulation of enzyme reactions using valence bond force fields and other hybrid quantum/classical approaches. *Chem. Rev. 93*, 2523–2544.
36. Luzhkov, V. B., and Åqvist, J. (2000) A computational study of ion binding and protonation states in the KcsA potassium channel. *Biochim. Biophys. Acta 1481*, 360–370.
37. Odintsova, T. I., Müller, E.-C., Ivanov, A. V., Egorov, T. A., Bienert, R., Vladimirov, S. N., Kostka, S., Otto, A., Wittmann-Liebold, B., and Karpova, G. G. (2003) Characterization and analysis of posttranslational modifications of the human large cytoplasmic ribosomal subunit proteins by mass spectrometry and Edman sequencing. *J. Protein Chem. 22*, 249–258.
38. Strader, M. B., VerBerkmoes, N. C., Tabb, D. L., Connelly, H. M., Barton, J. W., Bruce, B. D., Pelletier, D. A., Davison, B. H., Hettich, R. L., Larimer, F. W., and Hurst, G. B. (2004) Characterization of the 70S ribosome from *Rhodopseudomonas palustris* using an integrated "top-down" and "bottom-up" mass spectrometric approach. *J. Proteome Res. 3*, 965–978.
39. Chen, R., Mende, L., and Arfsten, U. (1975) The primary structure of protein L27 from the peptidyl-tRNA binding site of *Escherichia coli* ribosomes. *FEBS Lett. 59*, 96–99.
40. Suh, M.-J., Hamburg, D.-M., Gregory, S. T., Dahlberg, A. E., and Limbach, P. A. (2005) Extending ribosomal protein identifications to unsequenced bacterial strains using matrix-assisted laser desorption/ionization mass spectrometry. *Proteomics 5*, 4818–4831.

BI8001874